Int. J. Electrochem. Sci., 2 (**2007**) 444 - 461

International Journal of ELECTROCHEMICAL SCIENCE
www.electrochemsci.org

Spatiotemporal Oscillations in Peroxo-Molybdate Complexes in Acidic Solutions: 1. Impedance Measurements of $H_2Mo_2O_3(O\text{-}O)_4(H_2O)_2$

C.V.Krishnan[1, 2, *], *M. Garnett* [1], *B. Chu* [2]

[1]Garnett McKeen Lab, Inc., 7 Shirley Street, Bohemia, NY 11716-1735,USA
[2]Department of Chemistry, Stony Brook University, NY 11794-3400,USA
[*]E-mail: ckrishnan@notes.cc.sunysb.edu or newcode@aol.com

Received: 5 March 2007 / *Accepted:* 4 May 2007 / *Published:* 1 June 2007

Cyclic voltammetry data in the region 0 to - 0.4V using a static mercury drop electrode indicate a redox active peroxo-molybdate species in solutions obtained by dissolving the metal in 30% v/v H_2O_2. There was no observable colored species formation in this potential range. Admittance data at different frequencies suggest orientation effects of water molecules at or near the double layer. The admittance maximum near the double layer changeover region exhibits a small anodic shift on lowering the frequencies. Impedance measurements in aqueous $H_2Mo_2O_3(O\text{-}O)_4(H_2O)_2$ suggest spatiotemporal oscillations and the impedance loci observed in four quadrants near 0.1V is a characteristic of the Hopf bifurcation. This unique impedance is exhibited only in a narrow band potential. With increase in surface area the spatiotemporal periodicity becomes more efficient. The negative differential resistance observed, indicative of quantum mechanical resonant tunneling, points to the probable unique role of peroxide and molybdenum enzymes in global coupling to facilitate information transfer in biochemical processes.

Keywords: Spatiotemporal oscillations; Cyclic voltammetry; Admittance; Impedance; Peroxo-molybdate

1. INTRODUCTION

Giant polyoxomolybdate structure*s* have been obtained using polymers as 'templates' (actually reducing agents) and peroxo-molybdate species as a precursor [1]. The polyoxomolybdate units formed a continuous porous network that resembled the Linde type-A zeolite structure. The peroxo-molybdate species obtained by the dissolution of molybdenum in hydrogen peroxide have also been used to synthesize a variety of nanoparticles in the presence of polyethylene glycols or oxides as 'templates' via the sono-chemical route [2]. When the polymer concentration was less than that of the peroxo-molybdate, molybdenum oxide whiskers were obtained [3].

Molybdate interacts with hydrogen peroxide and forms a variety of peroxo complexes with 1 to 6 attached peroxide groups [4-6]. However, the dissolution of molybdenum in hydrogen peroxide has been reported to produce the solid $MoO_2(OH)(OOH)$ [7,8]. Later work on the peroxo-molybdate species produced by the reaction of molybdenum and hydrogen peroxide seemed to indicate the species in solution to be $H_2[Mo_2O_3(O\text{-}O)_4(H_2O)_2]$ [9], in agreement with the data on the oxidation of molybdenum at the anode to produce the species $[Mo_2O_3(O\text{-}O)_4]^{2-}$.

The majority of reported work on peroxomolybdates utilizes the reaction between simple molybdates and hydrogen peroxide [4,5]. However, cathodic electrodeposition of mixed molybdenum tungsten oxides as well as molybdenum oxides on transparent, conductive indium tin oxide (ITO)-coated glass substrates have been reported. The latter scheme used the peroxo-polymolybdotungstate and peroxo-molybdate solutions [10-12] prepared by the reaction of the respective metals and 30%v/v hydrogen peroxide and then by removing the excess peroxide using platinum black to achieve $[H_2O_2]/[\text{Mo or W}] \approx 1$.

Our previous work on nanoparticles of polyoxomolybdates[1-3] involved the synthesis by the reaction of peroxo-molybdate and polyethylene glycol (PEG) or polyethylene oxide (PEO). In these works, we found that the polyoxomolybdates were highly ordered and their morphologies could be partially controlled by the polymer chain-length. To understand the reaction mechanism of these reactions and to control the morphologies and particle-size of these polyoxomolybdates more precisely, one should know more about the nature of the substrate and the peroxo-molybdate species. We have investigated in detail the electrochemical characteristics of peroxo-molybdate species as well as the peroxide in the pH range 1-12. In the present electrochemical work, we report the nature of the peroxo-molybdate species in acidic solutions, below pH 2.

2. EXPERIMENTAL PART

Molybdenum powder (99.99%) was purchased from Aldrich (Milwaukee, WI). Fisher certified 30% v/v H_2O_2 was used for dissolving the molybdenum powder.

An EG & G PARC Model 303A SMDE tri electrode system (mercury working electrode, platinum counter electrode and Ag/AgCl (saturated KCl, reference electrode) along with Autolab eco chemie was used for cyclic voltammetric and electrochemical impedance measurements at 298 K. Distilled water was used for preparation of all solutions. To prepare 0.10 M solution (as Mo), two mL 30% hydrogen peroxide was carefully and slowly added drop by drop to 0.24 g molybdenum powder contained in an ice-cold 25 mL volumetric flask. After dissolution of the metal, the solution was made up to 25 mL. Some decomposition of the peroxide continued and the solution was kept for at least 24 hours before carrying out any electrochemical measurements. No other background electrolyte was used for the electrochemical measurements. The solutions were purged with N_2 for about 10 minutes before the experiment. Impedance measurements were carried out using about 7 mL solutions in the frequency range 1000 Hz to 25 mHz. The amplitude of the sinusoidal perturbation signal was 10 mV.

The spectrophotometric measurements were carried out using a Shimadzu UV-1650PC and 1mm quartz cells.

3. RESULTS AND DISCUSSION

3.1 Cyclic Voltammetry

Cyclic voltammetry could not be carried out with 0.05 M or 0.005M peroxo-molybdate (assumed as $H_2Mo_2O_3(O\text{-}O)_4(H_2O)_2$, immediately after preparation of the stock solution at 0.05M) because the mercury drop was not stable and was falling off during scanning. But after 1 day of preparation of the 0.05M stock, we were able to measure the cyclic voltammograms in 0.005 M solution. The results for three scans in the range 0 to -0.4 and back to 0 V as well as for the range 0.3 to – 0.4 and back to 0.3 V are shown in Figures 1 and 2. We chose this region for our investigation because a cathodic current increase had been observed in this region and this region was also a part of

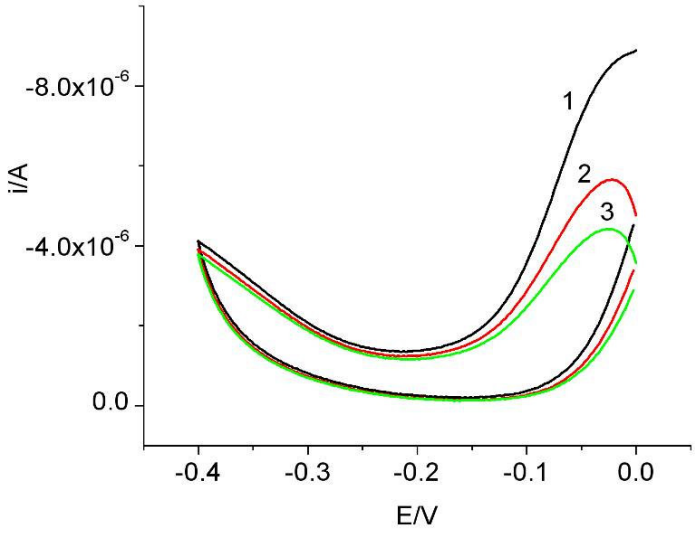

Figure 1. Cyclic voltammograms of 0.005 M $H_2Mo_2O_3(O\text{-}O)_4(H_2O)_2$, pH 1.87 after 1 day of preparation. A, scan 1; B, scan 2; C scan 3; scan rate 0.1 V/s; 0.0 to -0.4V

active region of MoO_3 films on conductive indium tin oxide (ITO)-coated glass [11-13]. The data indicate a cathodic peak at about -0.05 V. The results were nearly the same even when the scan was extended into positive potentials where mercury might begin to passivate. We observed the mercury to be shiny throughout the scans. However we did notice a decrease in the cathodic current with succeeding scans and this was consistent with earlier observations [11-13].

From the above results it is not obvious about the presence of multiple peroxo-molybdate species in solution. Or they must have similar redox characteristics at least in this limited potential range.

3.2 Admittance

A fresh sample of 0.005M $H_2Mo_2O_3(O\text{-}O)_4(H_2O)_2$ was used to measure admittance at different

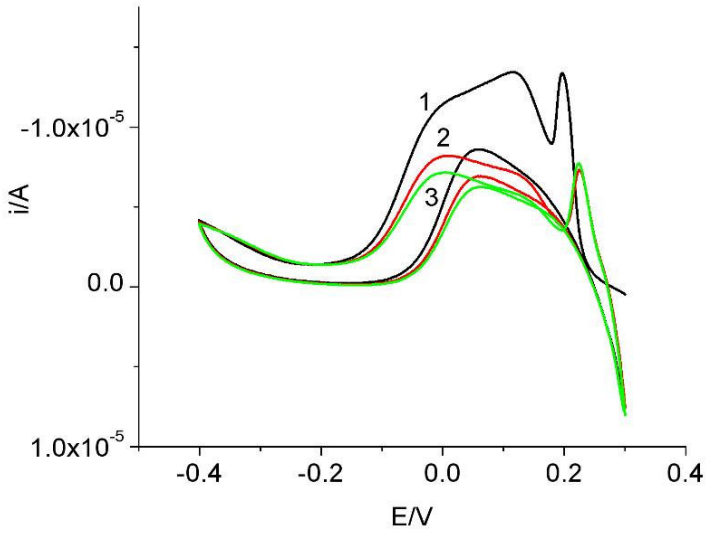

Figure 2. Cyclic voltammograms of 0.005 M $H_2Mo_2O_3(O\text{-}O)_4(H_2O)_2$, pH 1.87 after 1 day of preparation. A, scan 1; B, scan 2; C scan 3; scan rate 0.1 V/s; 0.3 to -0.4V

frequencies in the range -0.2 to +0.5 V. We had noticed that, in cyclic voltammograms, the passivation effects of the mercury electrode were not apparent even at 0.3V. We extended the current measurements to +0.5 V in order to locate the region of the double layer changeover. The admittance results are shown in Figure 3 for frequencies of 1000, 500, 250, 100, 50 and 25 Hz. It is interesting to note that admittance increased with lowering frequencies up to 100 Hz. Also it is apparent that at about 100 Hz, the peak at ~0.1 V began a slight anodic shift. Below 100Hz, the admittance decreased with a further decrease in frequency.

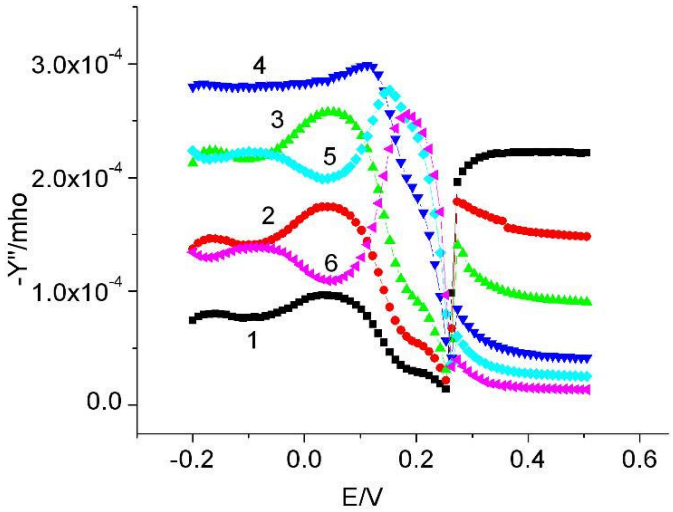

Figure 3. Admittance of 0.005 M $H_2Mo_2O_3(O\text{-}O)_4(H_2O)_2$, pH 1.87 after 2 days of preparation. 1, 1000 Hz; 2, 500 Hz; 3, 250 Hz; 4, 100 Hz; 5, 50 Hz; 6, 25 Hz

We had attributed the anodic shift in impedance with a decrease in frequency to the change in the orientation effects of water and to the change in the double layer structure when the potential of the mercury electrode changed from negative to less negative, to zero, and finally to positive. We had observed similar shifts even for alkali chlorides [14]. The admittance data indicate the passivation effects of mercury only after 0.25 V as was evident from a dramatic rise in admittance.

3.3 Differential Capacity

The double layer capacitance, generally obtained from differential capacitance measurements, should be independent of frequency. Our data, shown in Figure 4, exhibit a dispersion of capacitance with frequency, with the highest capacitance being for the lowest frequency. We have observed similar dispersions for alkali halides [14] as well as for isopolyoxomolybdates [15]. This dispersion could generally be attributed to the real surface with fractal characters instead of an ideal homogeneous electrode surface.

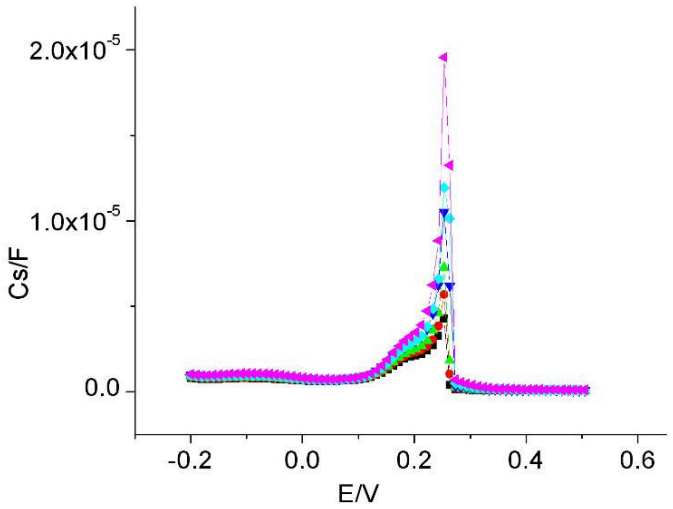

Figure 4. Differential capacitance of 0.005 M $H_2Mo_2O_3(O\text{-}O)_4(H_2O)_2$, pH 1.87 after 2 days of preparation, Frequencies used are 1000, 500, 250, 100, 50 and 25 Hz.

3.4 Semiconduction

The physico-chemical characterization of passive-film electrolyte junction or the study of semiconducting electronic properties of passive films is frequently carried out by measuring the differential capacitance of the junction as a function of electrode potential and frequency of the superimposed ac signal. Under the influence of a high electric field, cation and O^{2-} ion migration through the film results in oxide film growth and consequent passivation. For a p-type semiconductor, the film with a characteristic capacitance obeys the Mott-Schottky relationship:

$$C^{-2} = -[2/(q\varepsilon\ \varepsilon_0\ N_A)]\ (E\text{-}E_{FB} + kT/q)$$

Where C is the space charge capacitance; E is the electrode potential; ε is the vacuum permittivity (8.85×10^{-14} F/cm); ε_0, the dielectric constant of the specimen; q, the electron charge (1.602×10^{-19} Coulomb); k, the Boltzmann constant (1.38×10^{-23} J/K); T, the absolute temperature; N_A, the acceptor density; and E_{FB}, the flat band potential.

The Mott-Schottky plot shown in Figure 5 indicates an n-type behavior which is also a characteristic of MoO_3 [10]. Depending on the pH, we have observed both p-type as well as n-type behavior for isopolyoxomolybdates [15].

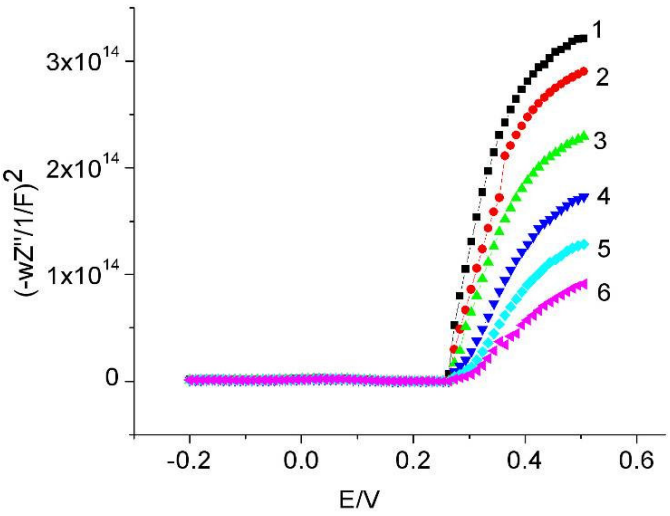

Figure 5. Mott-Schottky plot for 0.005 M $H_2Mo_2O_3(O\text{-}O)_4(H_2O)_2$, pH 1.87 after 2 days of preparation. 1, 1000 Hz; 2, 500 Hz; 3, 250 Hz; 4, 100 Hz; 5, 50 Hz; 6, 25 Hz

3.5 Impedance

The Nyquist plots or impedance spectra for 0.005M peroxo-molybdate solutions at potentials of – 0.2, -0.1, 0.0, and 0.1V, are shown in Figure 6 and that of 0.2 and 0.3V are shown in Figure 7.

The results in Figure 6 show a change from capacitive at -0.2 V to impedance loci in two quadrants exhibiting negative differential resistance at -0.1, and 0.0 volts, to impedance loci in four quadrants at 0.1 volt.

The impedance diagram shown in Figure 7 at 0.2 V exhibits two capacitive loops in the high and low frequency ranges and one inductive loop. The high frequency capacitive loop is associated with a charge transfer and a film effect. In corrosion studies, the resistance associated with the high frequency loop is effectively that of the charge transfer resistance and is often used in determining the corrosion current. Relaxation of mass transport in a solid phase (diffusional process) accounts for the low frequency capacitive loop. The inductive loop may be due to the relaxation of coverage due to an adsorbed intermediate. A further increase in potential to 0.3 V generates only two capacitive loops.

Figure 8 shows the impedance spectra for 0.005M peroxo-molybdate at 0.1V after 1 day of preparation. Some frequencies are included in the figure in order to get some idea of the frequencies at which the transitions in impedance loci take place from one quadrant to another quadrant.

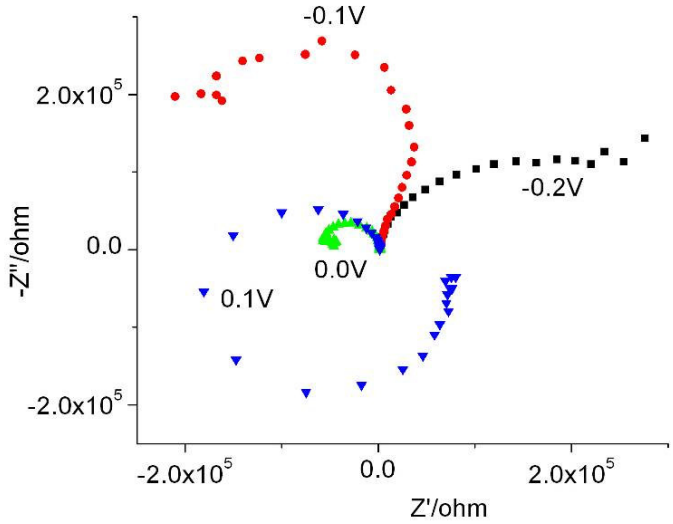

Figure 6. Nyquist plots for potential dependence of impedance of 0.005 M $H_2Mo_2O_3(O\text{-}O)_4(H_2O)_2$, pH 1.87 after 1 day of preparation.

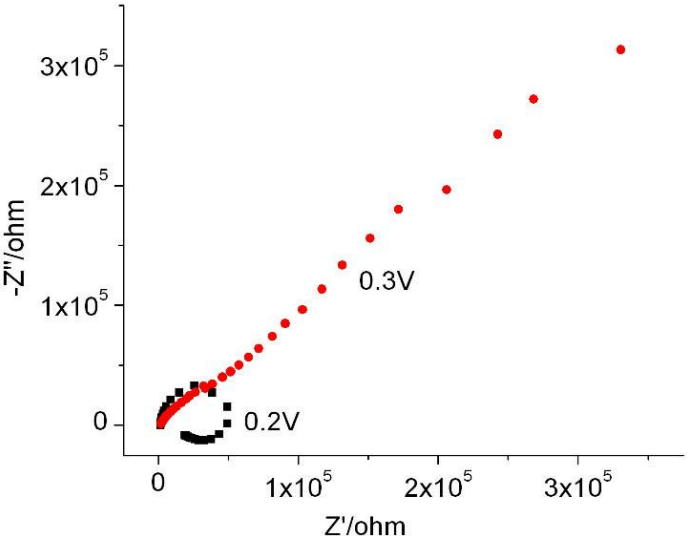

Figure7. Nyquist plots for potential dependence of impedance of 0.005 M $H_2Mo_2O_3(O\text{-}O)_4(H_2O)_2$, pH 1.87 after 1 day of preparation.

These results, especially the impedance loci occurring in four quadrants, as shown in Figures 6 and 8, are quite dramatic for this peroxo-molybdate system. Of course we have observed recently this kind of behavior for many biological molecules [16], a feature more commonly seen in only corrosion systems and often at very low frequencies[17-20]. This kind of impedance has also been predicted by theory [19, 21-22].

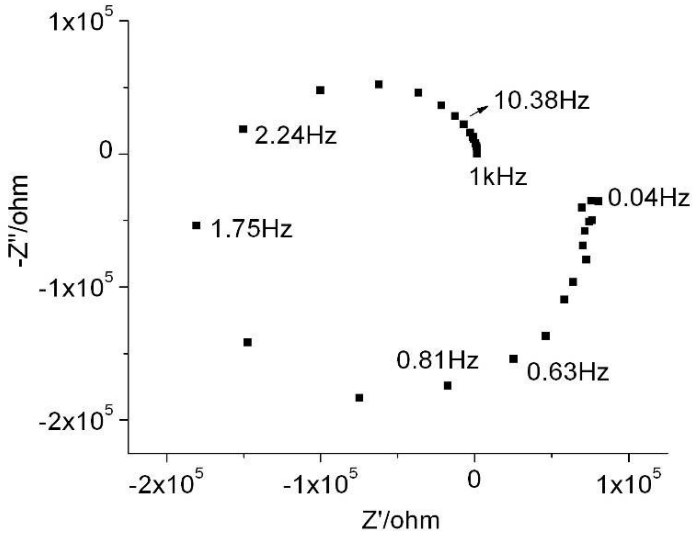

Figure 8. Impedance of 0.005 M $H_2Mo_2O_3(O\text{-}O)_4(H_2O)_2$, pH 1.87, after 1 day of preparation, 0.1V.

The modulus $|Z|$ and the phase angle Φ of $\mathbf{Z}(\omega)$ were obtained from $|Z| = [Z'^2 + Z''^2]^{1/2}$ and $\Phi = \tan^{-1}[Z''/Z']$, respectively. The phase angle is a balance between capacitive and resistive components. It is the angle between the directions of the real and imaginary components of Z at a given frequency. For pure resistance, $\Phi = 0$ and for pure capacitance, $\Phi = -90^o$. Thus, an approach to the capacitative behavior at low frequencies was identified provided that the phase angle was close to -90^o. The Bode plot complements the plot of the real and imaginary components of impedance in the complex plane. Whereas the impedance data at high frequencies are bunched together in Nyquist plots, the Bode plot shows the impedance behavior at all frequencies with equal weight and is often used for circuit analysis. For the sake of clarity, both the modulus and the phase angle are plotted separately and shown in Figures 9 and 10.

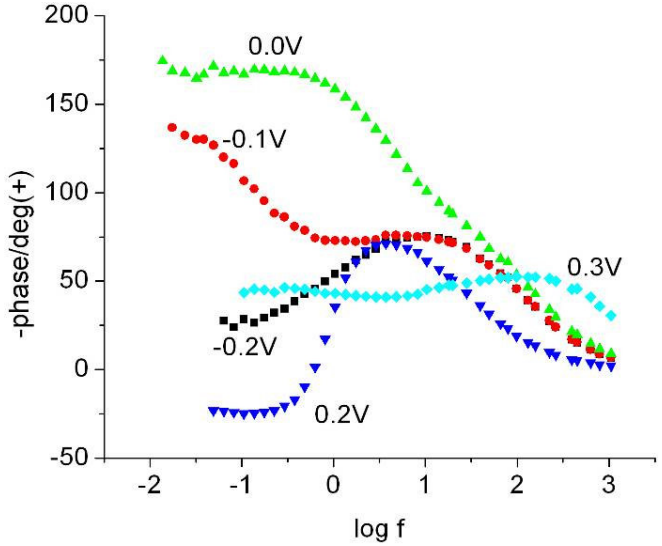

Figure 9. Potential dependence of phase angle (Bode plot) of 0.005 M $H_2Mo_2O_3(O\text{-}O)_4(H_2O)_2$, pH 1.87 after 1day of preparation.

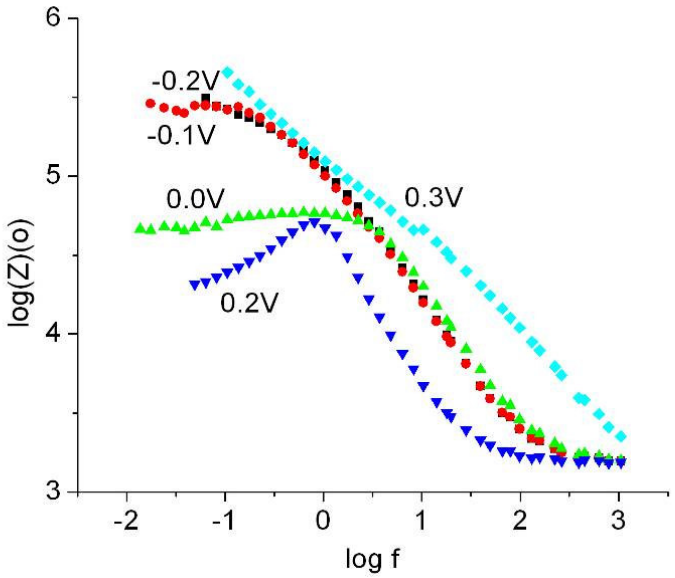

Figure 10. Potential dependence of impedance modulus (Bode plot) of 0.005 M $H_2Mo_2O_3(O\text{-}O)_4(H_2O)_2$, pH 1.87 after 1 day of preparation.

For the case with impedance loci occurring in four quadrants, the Bode plot is given in Figure 11.

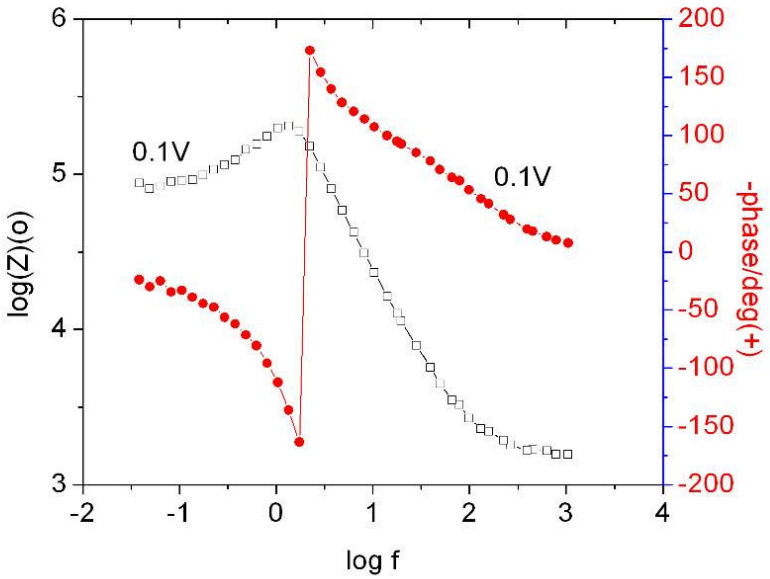

Figure 11. Bode plot of 0.005M $H_2Mo_2O_3(O\text{-}O)_4(H_2O)_2$, pH 1.87 after 1 day of preparation.

Stevenson and his colleagues [11-12] suggested the following reactions for the electrochemical deposition mechanism of molybdenum oxide thin films from peroxo-polymolybdate solution.
In the potential range +0.18 to + 0.02 V,

$$2[H_2MoO_4] + 2[H_3O^+] + 2e^- = Mo_2O_5(s) + 5H_2O \quad (1)$$

In the potential range +0.02 to -0.01 V,

$$[Mo_4O_9(O_2)_4]^{2-} + 2[H_2MoO_4] + 14[H_3O^+] + 12e^- = 2Mo_3O_8(s) + 23H_2O \quad (2)$$

and in the potential range -0.01 to -0.4 V

$$[Mo_2O_3(O_2)_4(H_2O)_2]^{2-} + [H_2MoO_4] + 12[H_3O^+] + 10e^- = Mo_3O_8(s) + 21H_2O \quad (3)$$

From quartz crystal microbalance data, they suggested the respective deposited products to be $Mo_2O_5.3H_2O$, $2(Mo_3O_8.H_2O)$ and $Mo_3O_8.H_2O$. They also suggested that $2[Mo_3O_8.H_2O]$ might be a mixture of several compounds, such as $Mo_6O_{16}.2H_2O \equiv Mo_4O_{11}.Mo_2O_5.2H_2O \equiv MoO_2(MoO_3)_3Mo_2O_5.2H_2O$. Our Mott-Schottky data suggest an n-type semi-conduction in this potential range and is consistent with the reported behavior MoO_3. This information may be coupled with the origin of electrochemical oscillations during hydrogen peroxide reduction on GaAs semiconductor electrodes [23] which is also an n-type semiconductor. Our impedance data in the third and fourth quadrant are much more reliable than the data for the GaAs. The only difference is that 1 M H_2SO_4 and 0.1 M H_2O_2 were used for the GaAs when compared to our milder conditions. However, we have a much more complex system and we are refraining from proposing a similar mechanism until more extensive investigations are carried out.

There are extensive studies of peroxide oscillations [23-30], mostly in high acid concentrations, and several types of oscillations have been identified. Of these, the number of impedance measurements was rather limited. We have extended peroxide studies in neutral solutions of alkali chlorides using a mercury electrode and applied it to understand biological phenomena, viz., the role of peroxide in evolution [31] and in Parkinson's disease [32].

The observed negative differential resistance was attributed to resonant tunneling [33] and was similar to the quantum mechanical tunneling taking place in tunnel diodes.

Our impedance spectra observed in four quadrants near 0.1 V is a characteristic of the Hopf bifurcation, which is an "excellent indicator of sustained nonlinear oscillations" [23]. Impedance data provide information on the instabilities or bifurcations and distinguish between saddle-node and Hopf bifurcations. The observed behavior in the third and fourth quadrants also suggests galvanostatic potential oscillations.

Similar to the explanation given for the passivation of copper [17], we attribute the impedance loci observed in four quadrants to the transition from the nonminimum phase-type to the minimum phase-type and correspond to the Hopf bifurcation under current control. We also observed the resonance-like maximum of the amplitude characteristic or impedance modulus indicative of harmonic relaxation along with the phase change behavior for the first order (discontinuous) nonminimum phase to the second order (continuous) minimum phase. Irrespective of the mercury drop size, the data suggested a Hopf bifurcation at this potential and the unique phase behavior reflecting the periodicities suggested global coupling.

3.6 Potential Dependence of Impedance Loci in Four Quadrants

The sensitive nature of the impedance loci occurring in 4 quadrants was investigated by carefully changing the potential at which the impedance was measured. The results are shown in Figures 12 and 13. We have not seen similar extensive studies before. Our results indicated that the impedance loci occurring in 4 quadrants was an optimum, in our case, at about 0.13-0.15 V. The impedance increased on both sides of this range. If we went much further on both sides, the results were entirely different, as shown in Figures 6 and 7.

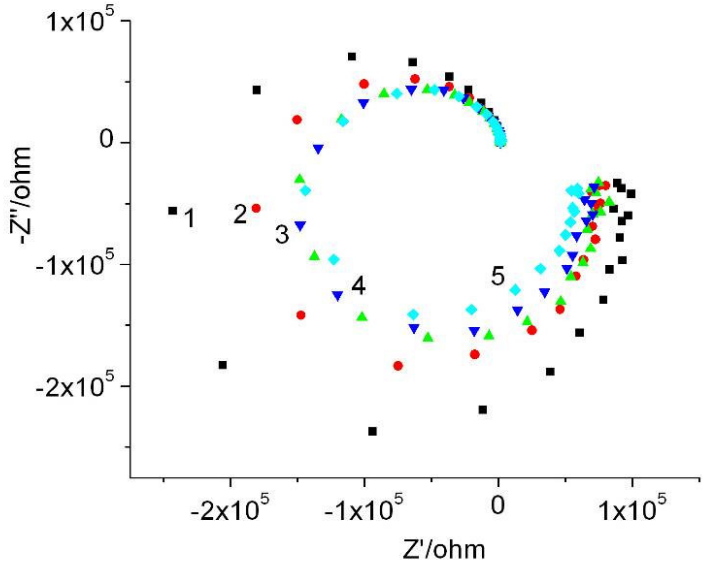

Figure 12. Impedance loci in four quadrants for 0.005 M $H_2Mo_2O_3(O\text{-}O)_4(H_2O)_2$, pH 1.87 after 1 day of preparation, potential dependence. 1, 0.05 V; 2, 0.10 V; 3, 0.13 V; 4, 0.14 V; 5, 0.15 V

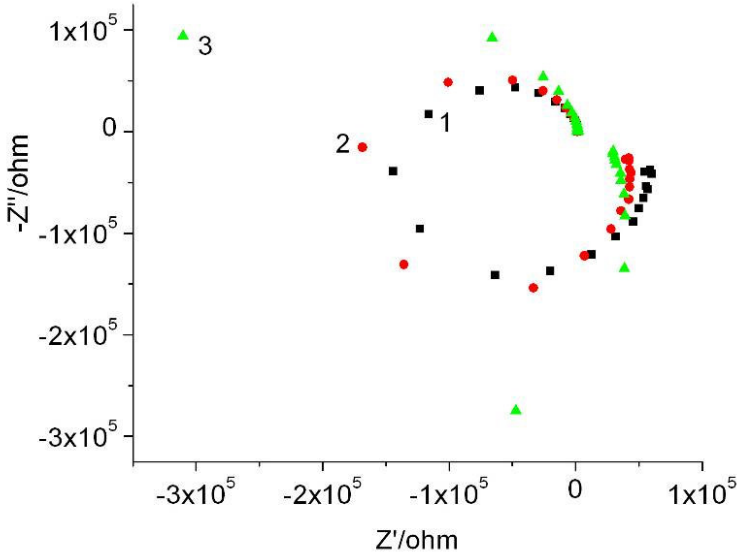

Figure 13. Impedance loci in four quadrants for 0.005 M $H_2Mo_2O_3(O\text{-}O)_4(H_2O)_2$, pH 1.87 after 1 day of preparation. 1, 0.15 V; 2, 0.16 V; 3, 0.17 V.

3.7 Equivalent Circuit Fit.

Several investigators have attempted to fit the observed impedance data in 4 quadrants using different models. For example Miller and Chen [34] used the circuit R(RC)(RQ)([R(RC)]C) where Q is the constant phase element to fit the sulfide oxidation on Ti/Ta_2O_5-IrO_2 electrodes. Sadkowski and his colleagues [17, 35] have attempted complex nonlinear least squares fits of suitable models and the three most common RC electrical equivalent circuit configurations, ladder, Voight-type and Maxwell-type, for anodic copper dissolution/passivation of copper in a solution of copper sulfate and sulfuric acid. Bojinov [36] has coupled growth/dissolution processes of a continuous film at its interface with the electrolyte, resulting in second order dynamic behavior of the metal/film/electrolyte system to explain the oxidation of metals in concentrated solutions and exhibiting peculiar shape in the complex impedance plane.

We have attempted in a modest way to fit the data for impedance loci occurring in two quadrants as well as in four quadrants. The fit for the two quadrant plot exhibiting negative differential resistance, shown in Figures 14 and 15, has the circuit R1(R2C1)(R3C2)(R4C3)(R5C4) and is similar to a transmission line model. The spectra at 0.1V exhibiting impedance loci in four quadrants, shown in Figures 16 and 17, may be fitted by two circuits, R1(Q1[R2(L1R3)]) and R1(R2Q1[R3Q2]), equally

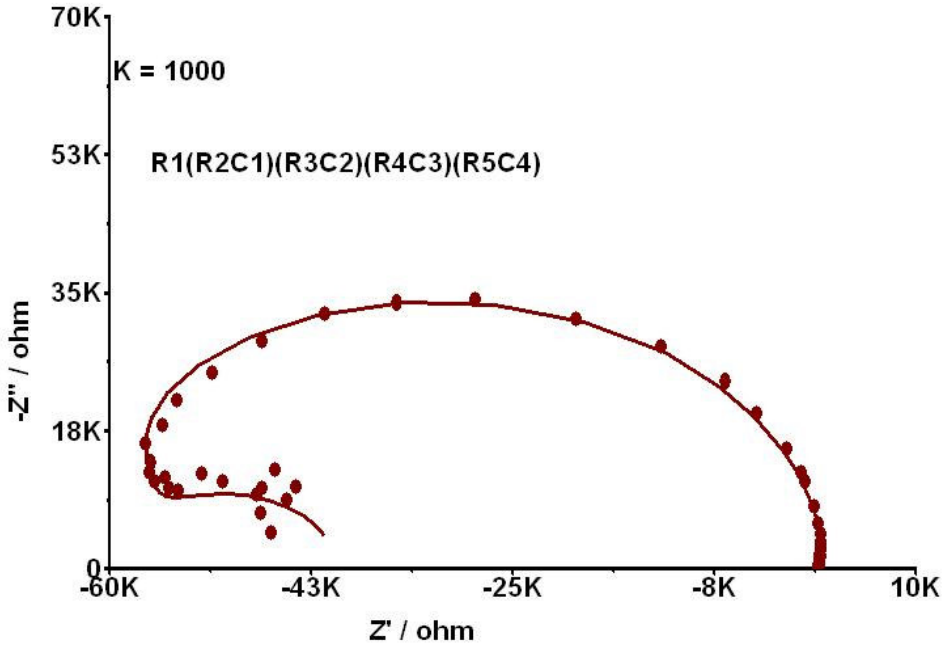

Figure14. Nyquist Plot at 0.0 V for 0.005 M $H_2Mo_2O_3(O\text{-}O)_4(H_2O)_2$, pH 1.87, 1000 – 0.038 Hz; the circuit R1(R2C1)(R3C2)(R4C3)(R5C4)

well. Here Q is the constant phase element which can be compared to a leaky capacitor. The constant phase element is introduced to explain the deviations of double layer capacitance from ideal behavior. Mercury gives the ideal smooth electrode surface compared to other electrodes which have a specific irregularity or roughness. The smoother and cleaner the electrode, the closer is Q to C.

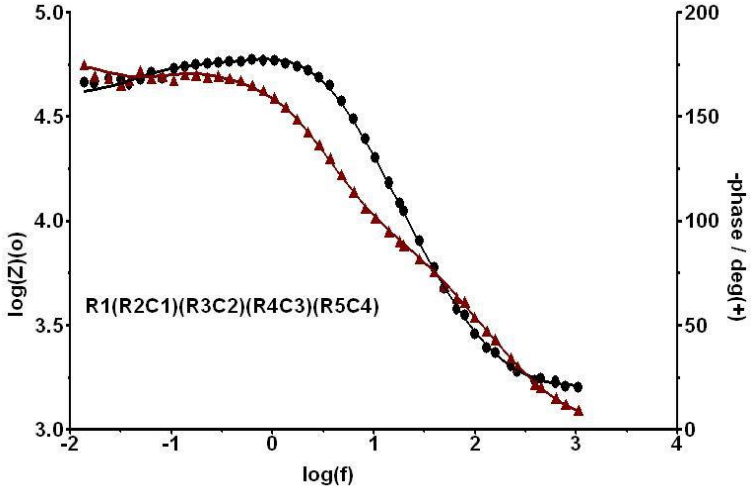

Figure15. Bode Plot at 0.0 V for 0.005 M $H_2Mo_2O_3(O\text{-}O)_4(H_2O)_2$, pH 1.87, 1000 – 0.038 Hz; the circuit R1(R2C1)(R3C2)(R4C3)(R5C4)

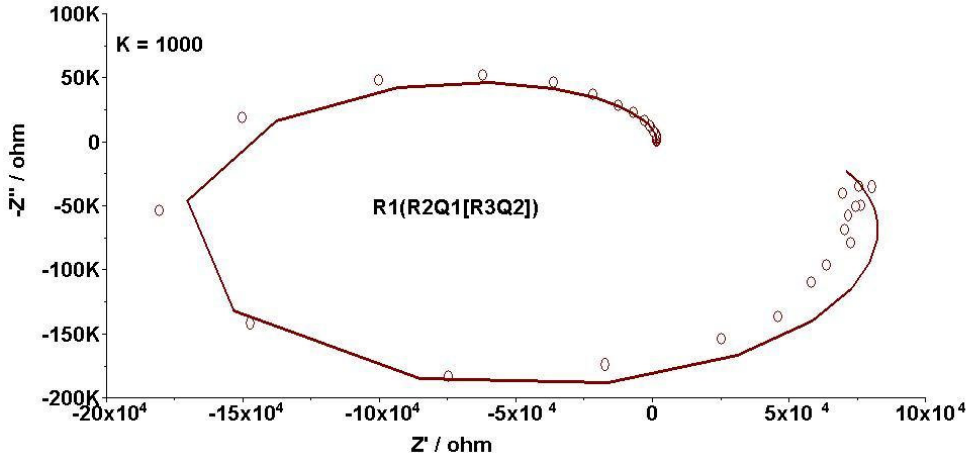

Figure 16. Nyquist Plot at 0.1 V for 0.005 M $H_2Mo_2O_3(O\text{-}O)_4(H_2O)_2$, pH 1.87, 1000 – 0.038Hz; the circuit R1(R2Q1[R3Q2)])

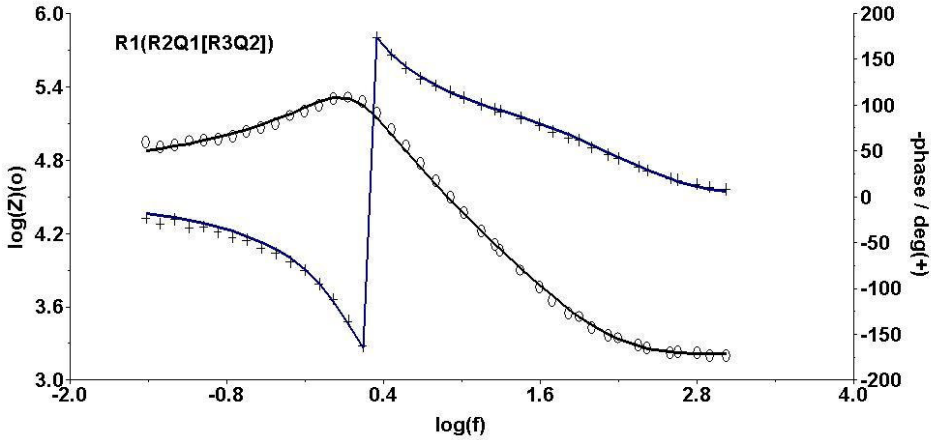

Figure17. Bode Plot at 0.1V for 0.005 M $H_2Mo_2O_3(O\text{-}O)_4(H_2O)_2$, pH 1.87, 1000 – 0.038 Hz; the circuit R1(R2Q1[R3Q2])

3.8 Stability of Experimental Data

The results for a set of 4 experiments in the frequency range 1000 Hz to 13 mHz are shown in Figure 18. It is remarkable that the impedance loci occurring in 4 quadrants is quite reproducible with little scatter. We have pointed out earlier [14] that depending on the nature of the curve chosen for reproducibility, one can manipulate the visual observation. If we were to use the Bode plots to show reproducibility, the scatter is much less than the one shown in Figure 18. The purpose of our experiment is to show the impedance loci in 4 quadrants rather than use that data for extensive calculations.

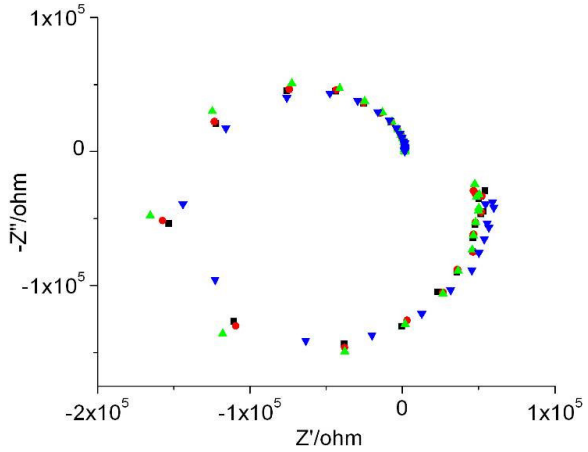

Figure 18. Four sets of impedance data for 0.005 M $H_2Mo_2O_3(O\text{-}O)_4(H_2O)_2$, pH 1.87 after 1day of preparation, 0.15V, 1000 Hz – 38 mHz.

3.9 Surface Area

It is extremely difficult to investigate the influence of surface area on the phenomenon of spatiotemporal periodicities using solid electrodes. In this respect, our approach of using mercury as the working electrode offers a great advantage. In the 303A SMDE trielectrode system, there are small, medium and large size select buttons. Also for impedance measurements, we can select the dispense

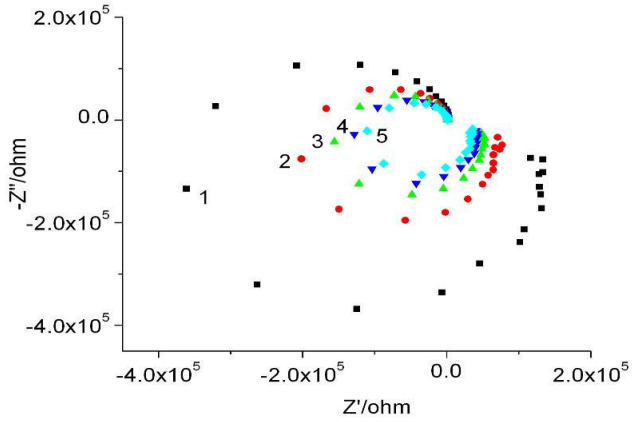

Figure 19. Impedance data for 0.005 M $H_2Mo_2O_3(O\text{-}O)_4(H_2O)_2$, pH 1.87 after 1 day of preparation, 0.15 V, 1000 Hz – 38 mHz; Surface in cm^2 for 1, 0.011; 2, 0.017; 3, 0.022; 4, 0.027; 5, 0.031

button to adjust the size of the drop by pushing the dispense button for the appropriate number of times before the mercury falls off. Thus, this system allows us to use a fresh surface each time. Our results are shown in Figure 19. It is clear that the larger the surface area the better the observed periodicity and the lower the observed impedance.

4. NATURE OF PEROXO-MOLYBDATE SPECIES IN SOLUTION

Even though there have been many investigations on peroxo-molybdate species in solution, there are only limited references about the nature of the species formed on the dissolution of molybdenum metal in hydrogen peroxide. For our experiments, molybdenum metal was dissolved in an excess 30% hydrogen peroxide. Since the resulting solution was highly acidic with a pH of about 1.5 for 1.0 M (as Mo) solution, the probable dissolution reaction could be [3,5]

$$2\ Mo + 10\ H_2O_2 \rightarrow H_2[(O)Mo(O\text{-}O)_2(O)(O\text{-}O)_2Mo(O)](H_2O)_2 + 7\ H_2O \qquad (4)$$

Hydrogen peroxide was involved in both the oxidation as well as coordination of molybdenum. The crystal structure of $K_2[Mo_2O_3(O_2)_4(H_2O)_2](H_2O)_2$ [37] indicated corner- sharing and edge-sharing polyhedra as in polymolybdates. Instead of the octahedral of polymolybdate, we had trigonal bipyramids with water molecules completing the seven coordination.

The species described in equation (4) is consistent with the equation suggested for the electrochemical oxidation of molybdenum [9] as

$$2\ Mo + 4\ H_2O_2 + 3\ H_2O \rightarrow [Mo_2O_3(O_2)_4]^{2-} + 14\ H^+ + 12\ e^-. \qquad (5)$$

We carried out some dilution experiments in order to observe whether there were any drastic changes in the solution behavior. The absorption spectra of the peroxo-molybdate used in our studies are shown in Figure 20 and the absorbances at 296 nm are shown in Figure 21.

The spectra indicate similar behavior. However the absorbance data indicate that Beer's Law is not obeyed, except in very narrow ranges and that dilution results in a shifting of equilibrium to other products of slightly different molar absorbances.

It has been suggested that the tetraperoxodimolybdate, $H_2Mo_2O_3(O_2)_4$ may be hydrolyzed to produce $H_2MoO_2(O_2)_2$ upon dilution [6].

$$H_2Mo_2O_3(O_2)_4 + H_2O = 2\ H_2MoO_2(O_2)_2 \qquad (6)$$

Polymerization of the 2: 1 (peroxide: Mo) peroxomolybdate has also been reported [38] at low pH values by the following reaction to produce a 1:1 tetraperoxotetramolybdate.

$$2[Mo_2O_3(O_2)_4(H_2O)_2]^{2-} + 2H_3O^+ = [Mo_4O_9(O_2)_4]^{2-} + 4H_2O_2 + 3H_2O \qquad (7)$$

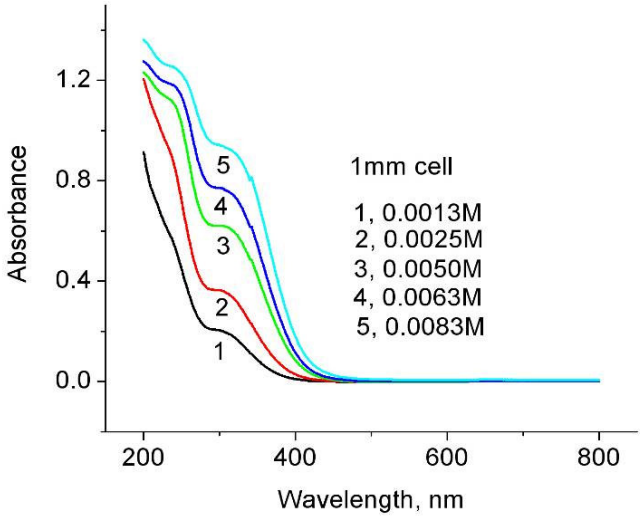

Figure 20. Absorption spectra of peroxo-molybdate obtained by dissolving Mo metal in 30% H_2O_2. Concentrations, M, are for $H_2Mo_2O_3(O\text{-}O)_4(H_2O)_2$

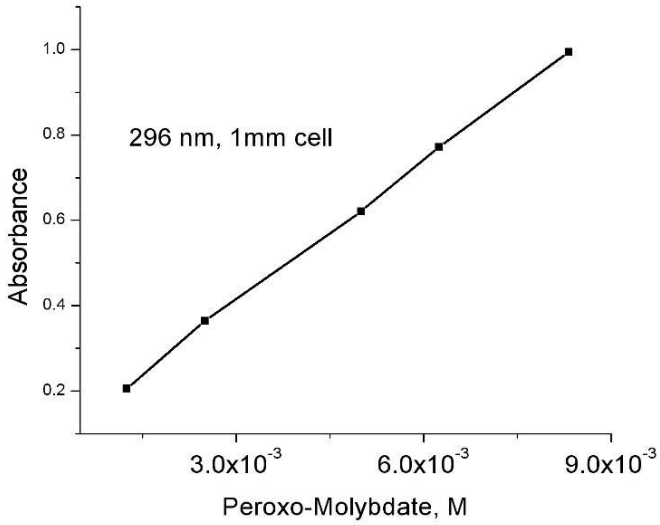

Figure 21. Absorbance data for $H_2Mo_2O_3(O\text{-}O)_4(H_2O)_2$ at varying concentrations

On dilution, this is hydrolyzed into the simpler diperoxodimolybdate, $H_2Mo_2O_5(O_2)_2$.

$$H_2Mo_4O_9(O_2)_4 + H_2O = 2H_2Mo_2O_5(O_2)_2 \quad (8)$$

Thus, in the beginning, when the peroxomolybdate solution is prepared by reacting Mo metal with an excess of peroxide, we may have $H_2Mo_2O_3(O_2)_4(H_2O)_2$, $H_2MoO_2(O_2)_2$, $H_2Mo_4O_9(O_2)_4$, and $H_2Mo_2O_5(O_2)_2$. The exact composition of this mixture is decided by dilution and the respective equilibria. The solution prepared by the above procedure has also been reported [5,11] to contain up to

40% molybdic acid (H_2MoO_4 or $MoO_2(OH)_2(H_2O)_2$) and this has been utilized to elucidate the mechanism of electrodeposition of molybdenum oxide from peroxomolybdate solutions [11].

Below pH 4 and with very low peroxide concentrations, higher order polymeric peroxo-species such as $[H_nMo_7O_{23}(O_2)]^{(6-n)-}$ and $[H_nMo_7O_{22}(O_2)_2]^{(6-n)-}$ (n = 0 to 3) are reported to exist in peroxo-molybdate solutions [39].

5. IMPLICATIONS TO BIOLOGICAL SYSTEMS

All living systems exhibit dynamical spatiotemporal periodicities [40]. The dynamical oscillations observed in the electrochemical passivation of metals and used as models for biological oscillations are attributed to the negative Faradaic impedance characteristics of the electrode [41]. Impedance data provide information on the instabilities or bifurcations and distinguish between saddle-node and Hopf bifurcations. There are many molybdenum enzymes as well as plenty of peroxide in all living systems. Thus our present results and the previous results with hydrogen peroxide [31, 32] suggest a unique role for peroxide in the global coupling to facilitate information transfer in biochemical processes.

6. CONCLUSIONS

Cyclic voltammetry data in the region 0 to - 0.4 V indicate a redox active peroxo-molybdate species in solution. There was no observable colored species formation in this potential range. Admittance data at different frequencies suggest orientation effects of water molecules at or near the double layer. Impedance measurements in aqueous peroxo-molybdate solutions of pH below 2 suggest spatiotemporal oscillations. The impedance loci observed in four quadrants near 0.1V is indicative of the Hopf bifurcation. This unique impedance was observed to exhibit only in a narrow band potential. With an increase in surface area, the spatiotemporal periodicity becomes more efficient. The frequency at which the negative differential resistance is observed also depends on the nature of the species suggesting the unique role of peroxide.

ACKNOWLEDGEMENT
Financial support of this work was provided by the Basic Energy Sciences, Department of Energy (DEFG0286ER45237.023)

References

1. T. Liu, Q. Wan, Y. Xie, C. Burger, L.Z. Liu, B. Chu, *J. Am. Chem. Soc*. 123, (2001)10966
2. J. Chen, C. Burger, C. V. Krishnan, B. Chu, *J. Am. Chem. Soc*. 127 (2005) 14140
3. C. V. Krishnan, J. Chen, C. Burger, B. Chu, *J. Phys. Chem*. B 110 (2006) 20182.
4. M.H. Dickman, M.T. Pope, *Chem. Rev*. 94, (1994) 569
5. K.H. Tytko, D. Gras, in H. Katscher, F. Schroder (Eds.), Gmelin Handbook of Inorganic Chemistry, Eighth ed., Mo Suppl., Springer Verlag, New York, Vol B(3b) (1989)
6. L.J. Csányi, *Transition Met. Chem*., 14 (1989) 298

7. K. Segawa, K. Ooga, Y. Kurusu, *Bull. Chem. Soc. Jpn*. 57, (1984) 2721
8. Y. Kurusu, *Bull. Chem. Soc. Jpn*. 54, (1981) 293
9. M.C. Chakravorti, S. Ganguly, and M. Bhattacharjee, *Polyhedron* 12, (1993) 55
10. L. Kondrachova, B.P. Hahn, G. Vijayaraghavan, R.D. Williams, K.J. Stevenson, *Langmuir*, 22 (2006) 10490
11. T.M. McEvoy, K.J. Stevenson, *J. Mater. Res*., 19 (2004) 429
12. T.M. McEvoy, K.J. Stevenson, *J. Mater. Res., Analytica Chimica Acta*, 496 (2003) 39
13. A. Guerfi, R.W. Paynter, Lê H. Dao, *J. Electrochem. Soc*., 142 (1995) 3457
14. C.V. Krishnan, M. Garnett, *Electrochimica Acta*, 51, (2006) 1541
15. C.V. Krishnan, M. Garnett, B. Hsiao, B. Chu, *Int. J. Electrochem. Sci*., 2 (2007) 29
16. C. V. Krishnan, M. Garnett, in "Passivation of Metals and Semiconductors, and Properties of Thin Oxide Layers", P. Marcus and V. Maurice (Editors), Elsevier, Amsterdam, (2006) 389
17. A. Sadkowski, M. Dolata, J.P. Diard, *J. Electrochem. Soc*., 151 (2004) E-20
18. M. Keddam, H. Takenouti, N. Yu, J. *Electrochem. Soc*., 132 (1985) 2561
19. D. D. Macdonald, *Electrochim. Acta*, 35 (1990) 1509
20. B.A. Boukamp, *J. Electrochem. Soc*., 142 (1995) 1885
21. C. Cao, *Electrochim. Acta*, 35 (1990) 837
22. D.D. MacDonald, E. Sikora, G. Engelhardt, *Electrochim. Acta*, 43 (1998) 87
23. M. T. M. Koper, D. Vanmaekelbergh, *J. Phys. Chem*., 99 (1995) 3687
24. S. Fukushima, S. Nakanishi, K. Fukami, S. Sakai, T. Nagai, T. Tada, and Y. Nakato, *Electrochemistry Communications*, **7**, (2005) 411
25. Y. Mukouyama, S. Nakanishi, H. Konishi, Y. Ikeshima, Y. Nakato, *J. Phys. Chem*., B 105 (2001) 10905
26. G. Flätgen, S. Wasle, M. Lübke, C. Eickes, G. Radhakrishnan, K. Doblhofer, G. Ertl, *Electrochimica Acta*, 44 (1999) 4499
27. G. Neher, L. Pohlmann, H. Tributsch*, J. Phys. Chem*., 99 (1995) 17763
28. S. Štrbac, R. R. Adžić, *J. Electroanal. Chem*., 337 (1992) 355
29. N. Fetner and J. L. Hudson, *J. Phys. Chem*., 94 (1990) 6506
30. J. J. Lingane and P. J. Lingane, *J. Electroanal. Chem*., 5, (1963) 411
31. M. Garnett, C. V. Krishnan, B. Chu, 209th Meeting of Electrochemical Society, Denver, Colorado, 2006
32. C. V. Krishnan, M. Garnett, B. Chu, 209th Meeting of Electrochemical Society, Denver, Colorado, 2006
33. J.A. Switzer, C-J. Hung, L-Y. Huang, E.R. Switzer, D.R. Kammler, T.D. Golden, E.W. Bohannan, *J. Am. Chem. Soc*., 120 (1998) 3530
34. B. Miller, A. Chen, *Electrochimica Acta*, 50 (2005) 2203
35. A. Sadkowski*, J. Electroanal. Chem*., 573 (2004) 241
36. M. Bojinov, *J. Electroanal. Chem*., 405 (1996) 15
37. R. Stomberg*, Acta Chemica Scandinavica*, 22 (1968)1076
38. E. Richardson, *J. Less-Common Met*. 2 (1960) 360
39. O.W. Howarth, L. Petttersson, I. Anderson, in Polyoxometalate Chemistry from Topology via Self-Assembly to Applications, M.T. Pope, A. Muller, Eds., Kluwer, Dordrecht, (2001) 145
40. R. J. Field and L. Gyorgyi, Editors in "Chaos in Chemistry and Biochemistry", World Scientific Publishing Co., NJ 07661, USA, 1993
41. M.T.M. Koper, *Adv. Chem. Phys*., 92(1996) 161